E 3 Donors for Quantum Information Processing

M. S. Brandt
Walter Schottky Institut
Technische Universität München

Contents

Corrected reprint from
Spintronics – From GMR to Quantum Information,
Lecture Notes of the 40th Spring School of the Institute of Solid-State Research, Forschungszentrum Jülich,
ed. by S. Blügel, D. Bürgler, M. Morgenstern, C. M. Schneider and R. Waser, 2009

1 The case for silicon

The quest to realize hardware for quantum information processing, and in particular for quantum computation, has motivated many research groups to assess the usability of the physical objects they study for this purpose. This has brought together experimentalists working on rather diverse topics such as ion traps, quantum optics, superconducting electronics and semiconductor physics with theoreticians developing quantum algorithms and studying decoherence processes.

It is beyond the scope of this brief introduction into donor-based qubits to fully compare the benefits and challenges of the different quantum bits or qubits investigated so far. DiVincenzo has compiled a set of requirements which can be used as a guideline for such a comparison [1]. In particular, a scalable physical system with well characterized qubits is needed, with the ability to initialize and to measure them. A universal set of quantum gates, allowing the manipulation of a single qubit as well as the controlled interaction of two qubits is required. In addition, the time needed to perform gate operations has to be much smaller than the time during which the qubits lose their coherence. And finally, one should be able to transmit qubits between distant locations. So far, nuclear spins have been used most successfully to demonstrate that quantum algorithms really work [2]. However, these groundbreaking studies have been limited to small molecules with little more than a handful of spins and qubits. Magnetic moments, both associated with nuclei and electrons, are also present in semiconductors. It is therefore an interesting question whether scalable spin-based qubit systems can be realized in semiconductors, where in conventional microelectronics memory chips with more than 10^9 classical bits can be fabricated.

Several different approaches exist to form electron spin qubits in semiconductors, such as the spins of electrons in electrostatically-defined or self-organized quantum dots, the spins of electrons bound to donors or the spins of electrons bound to defects or defect complexes. Useful nuclear spin qubits in semiconductors are in particular the nuclears spins of the donor atoms or of the atoms involved in defects and, if the semiconductor host material can be isotopically engineered, also the nuclear spins of the host atoms. To somewhat summarily go through the DiVincenzo criteria for spins in semiconductors, all qubit concepts mentioned above have been realized, and single qubit read-out, single qubit manipulation via magnetic resonance [3] as well as controlled coupling of qubits has been demonstrated for many of the concepts, but certainly not all. A general challenge of all solid state-based qubits including spins is the transfer of qubit states over long distances and it has to be noted that in this respect all solid-state qubit systems have not yet lived up to their originally presumed promise.

Which solid-state spin qubit system should therefore be pursued? As has been noted by DiVincenzo, it may still be counterproductive to even ask this question at the present stage of research into semiconductor qubits [1]. To identify possible strengths of particular spin systems, let us however compare the times T_1 and T_2 of different spin systems in semiconductors which characterize the lifetime and the coherence time of qubits, respectively. T_1 is used in the Bloch equations to describe the relaxation of a magnetization back to the equilibrium. During this relaxation, the energy of the spin system changes and therefore this relaxation is also called spin-lattice relaxation. In contrast, T_2 accounts for processes which do not change the energy of the spin system such as spin-spin scattering.

For electron spins in electrostatically-defined quantum dots fabricated in III-V compound semiconductor heterostructures, a T_1 of 0.85 ms [4] and values for T_2 longer than 1 μs [5] have been reported at temperatures of about 100 mK. For electrons in self-organized III-V quantum dots, values for T_1 up to 20 ms have been found at 1 K [6]. This comparison has to be taken with a grain of salt, since both T_1 and T_2 very sensitively depend on the temperature and the magnetic field.

The most systematic investigation of the spin properties of donors has been performed in silicon. For the electron spin of phosphorus donors at 1.25 K, a T_1 of 3000 s has been reported [7]. As in the case of quantum dots, a strong dependence on the temperature T is observed and T_1 is found to vary proportional to T^{-7} between 2.5 and 4.2 K. As expected for spin-spin interaction, T_2 is found to depend on the P concentration and T_2 times as long as 4 ms have been observed at 7 K [8]. For the corresponding nuclear spin I=1/2 of the ^{31}P nucleus, a T_1 exceeding 10 hours was reported at 1.25 K [7]. More recently, values of T_2 for phosphorus nuclear spins of nearly 2 s have been measured at 7 K [9].

Although the wave functions of electrons in quantum dots and at donors differ dramatically and therefore a direct comparison of the relevant relaxation and decoherence mechanisms is difficult, there is one key difference in the host materials: As shown in Tab. 1, all stable isotopes of the elements of groups III and V of the periodic table have a nuclear spin. In contrast, the elements of group IV have stable isotopes with no nuclear spin. In fact, isotopes of group-IV elements with a nuclear magnetic moment have a low abundance, so that Si crystals with a natural isotope composition contain only about 4.7 % of ^{29}Si with I=1/2. Therefore, cross relaxation processes between the electron and the nuclear spin systems are less important in C, Si and Ge and can in particular be engineered by artificially changing the isotope composition, e.g. by either reducing or enhancing the ^{29}Si concentration in Si crystals. Detailed experiments as a function of the isotope composition indeed show that the presence of ^{29}Si decreases both the effective T_1 and T_2 of donors in silicon [8][10].

Group III			Group IV			Group V		
^{10}B	3	19.9 %	^{12}C	0	98.9 %	^{14}N	1	99.6 %
^{11}B	3/2	80.1 %	^{13}C	1/2	1.1 %	^{15}N	1/2	0.4 %
^{27}Al	5/2	100 %	^{28}Si	0	92.2 %	^{31}P	1/2	100 %
			^{29}Si	1/2	4.7 %			
			^{30}Si	0	3.1 %			
^{69}Ga	3/2	60.1%	^{70}Ge	0	21.2 %	^{75}As	3/2	100 %
^{71}Ga	3/2	39.9 %	^{72}Ge	0	27.7 %			
			^{73}Ge	9/2	7.7 %			
			^{74}Ge	0	35.9 %			
			^{76}Ge	0	7.4 %			
^{113}In	9/2	4.3 %	^{119}Sn	1/2	8.6 %	^{121}Sb	5/2	57.2 %
^{115}In	9/2	95.7 %	^{120}Sn	0	32.6 %	^{123}Sb	7/2	42.8 %
			and eight other isotopes					

Tab. 1: *Stable isotopes of the elements of the main groups III, IV and V, their nuclear spin and natural abundance.*

The above discussion, to my opinion, is a clear case for using group-IV elements to construct the host material for spin qubits. Indeed, first experiments are under way to transfer the

investigation of spins in electrostatically-defined quantum dots to Si/SiGe heterostructures [11] with the ultimate aim of nuclear-spin free heterostructures such as ^{28}Si/^{28}Si^{70}Ge. However, a particular benefit of group-V donors as qubits in contrast to electrons in quantum dots is the nuclear spin of the donor atom, which due to the very long T_1 and T_2 times given above might very conveniently be used as qubit memory.

Why silicon, and not diamond, where the so-called NV-center, a defect complex formed by a N donor and a vacancy, shows T_2 times of up to 240 μs at room temperature [12][13] and single spin read-out has been demonstrated? This question is more difficult to answer. Read-out of the NV-center is performed optically. In contrast, most read-out concepts investigated for donors in silicon are based on electrical measurements which in principle are more easily integrated into existing microelectronics, incidentally also based on Si, rather than optical detection schemes. The comparatively shallow donor level of P in Si of 45 meV below the conduction band, on the other hand, is easily thermally ionized, so that in bulk Si the use of P donors for quantum information processing will be limited to temperatures below 30 K. In nanostructures, however, the donor becomes deeper and could therefore be used at higher temperatures as well. Another possibility to increase the accessible temperature range could be double donors such as Se, which have a much deeper donor level.

In conclusion, the possibility to isotopically engineer group-IV materials and the long spin lifetimes and coherence times of nuclear spins in these materials render donor states or donor-defect complexes in C, Si, Ge, their alloys and heterostructures well worth being studied as qubits. After a brief summary of the theoretical description of the interaction of electron spins with nuclear spins, we will discuss two concepts for donor-based quantum logic devices and methods used to position single donor atoms. Finally, we will look into experiments on how to read-out the spin state of phosphorus donors via spin-to-charge conversion at the Si/SiO_2-interface.

2 Coupling of electron spins and nuclear spins

2.1 The spin Hamiltonian

The analysis of the complete Hamiltonian of donor or defect states in a semiconductor matrix is very complex. For a description of the spin properties only, this difficulty is circumvented by the concept of a spin Hamiltonian $\boldsymbol{H}$, which explicitly includes only spin states and operators, e.g.

$$\boldsymbol{H} = \mu_B \vec{B} \hat{g} \vec{\boldsymbol{S}} + \vec{\boldsymbol{S}} \hat{D} \vec{\boldsymbol{S}} + \vec{\boldsymbol{S}} \hat{A} \vec{\boldsymbol{I}}, \tag{1}$$

with the Bohr magneton μ_B = 9.274015×10^{-28} J/G, the magnetic field $\vec{B}$, and the electronic and nuclear spin operators $\vec{\boldsymbol{S}}$ and $\vec{\boldsymbol{I}}$. The parameters $\hat{g}$, $\hat{D}$, and $\hat{A}$ are in general spatially anisotropic matrices with at least the symmetry properties of the orbital wave function of the paramagnetic state. By convention, $\hat{g}$ represents the Zeeman interaction of the electronic spin $\vec{\boldsymbol{S}}$ with the magnetic field, $\hat{D}$ the fine structure interaction, and $\hat{A}$ the hyperfine interaction between the electronic and a nuclear spin.

To separate the spin and real space operators in such a way, it must be assumed that a ground state wave function can be factorized as the product of a spin state and some non-degenerate many-particle orbital wave function. The time-independent Schrödinger equation $\boldsymbol{H}|\psi\rangle = E_\psi|\psi\rangle$ for the spin states $|\psi\rangle$ and their eigenenergies E_ψ can often be solved

analytically. In more complex spin systems, they must be calculated numerically or via perturbation theory. The orbital parts of the wave function and spatial operators like crystal field and spin-orbit interaction are integrated out and appear only implicitly in the spin Hamiltonian via effective numerical parameters such as the effective g-tensor $\hat{g}$, whose deviation from the free electron's g-factor g_0=2.002319 stems from spin-orbit coupling $\boldsymbol{H}_{so} = \lambda \vec{\boldsymbol{L}}\vec{\boldsymbol{S}}$ treated by second order perturbation theory [14]. The form of the spin Hamiltonian is found either ad hoc, i.e. phenomenologically, motivated by symmetry considerations, or by a perturbative expansion of the full Hamiltonian [15].

2.2 Matrix representation

Spin operators $\vec{\boldsymbol{S}}$, which are used in various combinations to form the spin Hamiltonian, have the general quantum-mechanical properties of an angular momentum [16]

$$\vec{\boldsymbol{S}}^2 \left|m\right\rangle = S(S+1)\left|m\right\rangle \tag{2}$$

$$\boldsymbol{S}_z \left|m\right\rangle = m\left|m\right\rangle \tag{3}$$

$$\boldsymbol{S}_\pm \left|m\right\rangle = \left(\boldsymbol{S}_x \pm i\boldsymbol{S}_y\right)\left|m\right\rangle = \sqrt{S(S+1)-m(m\pm 1)}\left|m\pm 1\right\rangle \quad . \tag{4}$$

These equations are valid for spin S = 1/2 electrons as well as for many-electron systems with higher values of S. A set of basis vectors for the 2S+1-dimensional spin space is defined by unit vectors for the orthonormal states $\left|m\right\rangle$ with the eigenvalues m=−S, … , S of the operator $\boldsymbol{S}_z$. The spin operators $\boldsymbol{S}_{x,y,z}$ take the form of matrices with dimension (2S + 1) × (2S + 1). For a spin-1/2 system, these are the well-known Pauli matrices, which may be combined in a vector notation of operators to $\vec{\boldsymbol{S}} = \left(\boldsymbol{S}_x, \boldsymbol{S}_y, \boldsymbol{S}_z\right)$ to describe the anisotropic properties of spins. The matrix forms of the spin operators for all higher values of S are defined by Eqs. (2) to (4). In short form, all non-zero matrix elements $\left\langle n\left|\boldsymbol{S}_{x,y,z}\right|m\right\rangle$ of the operators $\boldsymbol{S}_{x,y,z}$ can be summarized as

$$\left\langle n\left|\boldsymbol{S}_x\right|m\right\rangle = \delta_{n,m\pm 1}\frac{1}{2}\sqrt{S(S+1)-m(m\pm 1)} \tag{5}$$

$$\left\langle n\left|\boldsymbol{S}_y\right|m\right\rangle = \mp\delta_{n,m\pm 1}\frac{i}{2}\sqrt{S(S+1)-m(m\pm 1)} \tag{6}$$

$$\left\langle n\left|\boldsymbol{S}_z\right|m\right\rangle = \delta_{n,m} m \quad . \tag{7}$$

With a spin Hamiltonian built from linear combinations of such matrix operators, the Schrödinger equation becomes a simple matrix equation, whose eigenvalues can be calculated from the characteristic polynomial $\det\left(\boldsymbol{H}\text{-}\boldsymbol{1}E_i\right) = 0$, where $\boldsymbol{1}$ is the unity matrix, and $E_i(\vec{B})$ is one of the eigenvalues of the matrix equation. The corresponding eigenvector $\left|\psi_i\right\rangle$ defines the spin eigenstate for E_i as a linear combination $\left|\psi_i\right\rangle = \sum_m \alpha_{im}\left|m\right\rangle$ of the pure basis vectors of $\boldsymbol{S}_z$. These basis vectors $\left|m\right\rangle$ of $\boldsymbol{S}_z$ are usually the eigenstates of the spin Hamiltonian in the limit of very high magnetic fields along the z-axis, where all other perturbations can be neglected.

A system of several spins, e.g. one electronic spin S and one nuclear spin I, requires a total of $(2S + 1)\otimes(2I + 1)$ orthogonal eigen-vectors. The orthonormal basis vectors $\left|m_s, m_i\right\rangle$ of the product space may again be organized as unit vectors, now with a combined index (m_s,m_i),

which takes all values (−*S*,−*I*), (−*S*,−*I*+1), … , (*S*,*I*). The matrix elements $\langle n_s, n_i | \boldsymbol{S}_{x,y,z}, \boldsymbol{I}_{x,y,z} | m_s, m_i \rangle$ of the electronic and nuclear spin operators are defined according to Eqs. (5) to (7) also in this product space. The operators $\boldsymbol{S}_{x,y,z}$ leave the nuclear spin states unaffected and are represented by the unity matrix elements $\delta_{ni,mi}$ for the nuclear spin, and vice versa $\boldsymbol{I}_{x,y,z}$ leave the electronic spin states unaffected and are represented by the unity matrix elements $\delta_{ns,ms}$ for the electronic spin, i.e.

$$\langle n_s, n_i | \boldsymbol{S}_{x,y,z} | m_s, m_i \rangle = \delta_{ni,mi} \langle n_s | \boldsymbol{S}_{x,y,z} | m_s \rangle \tag{8}$$

$$\langle n_s, n_i | \boldsymbol{I}_{x,y,z} | m_s, m_i \rangle = \delta_{ns,ms} \langle n_i | \boldsymbol{I}_{x,y,z} | m_i \rangle \tag{9}$$

with the operators on the right-hand side as defined in Eqs. (5) to (7).

2.3 Diagonalization procedures

The spin Hamiltonian matrix needs to be diagonalized in order to obtain its eigenenergies E_i and eigenvectors $|\psi_i\rangle$ [17]. In cases where it is not possible to solve the matrix Schrödinger equation analytically, approximate solutions from perturbation theory, or exact numerical solutions for one set of matrix elements at a time must be obtained. These calculations are somewhat simplified, if the magnetic field is oriented along the *z*-axis of the spin Hamiltonian, as typically the Zeeman term dominates the eigenenergies of the spin. For other orientations of the magnetic field, this can be achieved by a rotation of the coordinate system of the spin operators $\vec{\boldsymbol{S}}' = \hat{R}\vec{\boldsymbol{S}}$ [17]. In the new coordinate system, the other possible interactions then introduce only small off-diagonal elements to the spin Hamiltonian.

The case of a phosphorus donor with *S*=1/2 and *I*=1/2, $\boldsymbol{H}$ can be solved analytically by inspection. Neglecting the weak nuclear Zeeman interaction, the spin Hamiltonian is

$$\boldsymbol{H} = \mu_B \vec{B}\hat{g}\vec{\boldsymbol{S}} + \vec{\boldsymbol{S}}\hat{A}\vec{\boldsymbol{I}} = \mu_B \vec{B}\hat{g}\vec{\boldsymbol{S}} + A\left(\boldsymbol{S}_x\boldsymbol{I}_x + \boldsymbol{S}_y\boldsymbol{I}_y + \boldsymbol{S}_z\boldsymbol{I}_z\right) \tag{10}$$

with the external magnetic field $\vec{B} = (0,0,B)$ along the *z*-direction, the isotropic g-factor $\hat{g} = \boldsymbol{1}g$, and the isotropic hyperfine interaction $\hat{A} = \boldsymbol{1}A$. The basis vectors $|m_s, m_i\rangle$ of the 4-dimensional product basis of $\boldsymbol{S}_z$ and $\boldsymbol{I}_z$ in this example are

$$\left|\frac{1}{2},\frac{1}{2}\right\rangle = \begin{pmatrix}1\\0\\0\\0\end{pmatrix}, \quad \left|\frac{1}{2},-\frac{1}{2}\right\rangle = \begin{pmatrix}0\\1\\0\\0\end{pmatrix}, \quad \left|-\frac{1}{2},\frac{1}{2}\right\rangle = \begin{pmatrix}0\\0\\1\\0\end{pmatrix}, \quad \left|-\frac{1}{2},-\frac{1}{2}\right\rangle = \begin{pmatrix}0\\0\\0\\1\end{pmatrix}. \tag{11}$$

The matrix form of this spin Hamiltonian is given by

$$\boldsymbol{H} = \begin{pmatrix} +\frac{\mu_B Bg}{2} + \frac{A}{4} & 0 & 0 & 0 \\ 0 & +\frac{\mu_B Bg}{2} - \frac{A}{4} & \frac{A}{2} & 0 \\ 0 & \frac{A}{2} & -\frac{\mu_B Bg}{2} - \frac{A}{4} & 0 \\ 0 & 0 & 0 & -\frac{\mu_B Bg}{2} + \frac{A}{4} \end{pmatrix}. \tag{12}$$

The off-diagonal elements $A/2 << \mu_B Bg$ can be neglected for small hyperfine couplings compared to the Zeeman interaction. In this case, Eq. (12) is already approximately diagonal, which means that the diagonal elements and the basis vectors of Eq. (11) are a first-order approximation to the eigenenergies and eigenvectors of the system. In this regime, both *S* and *I* are quantized along the external magnetic field. These first-order eigenenergies are shown as a function of *B* in the energy diagram of Fig. 1a).

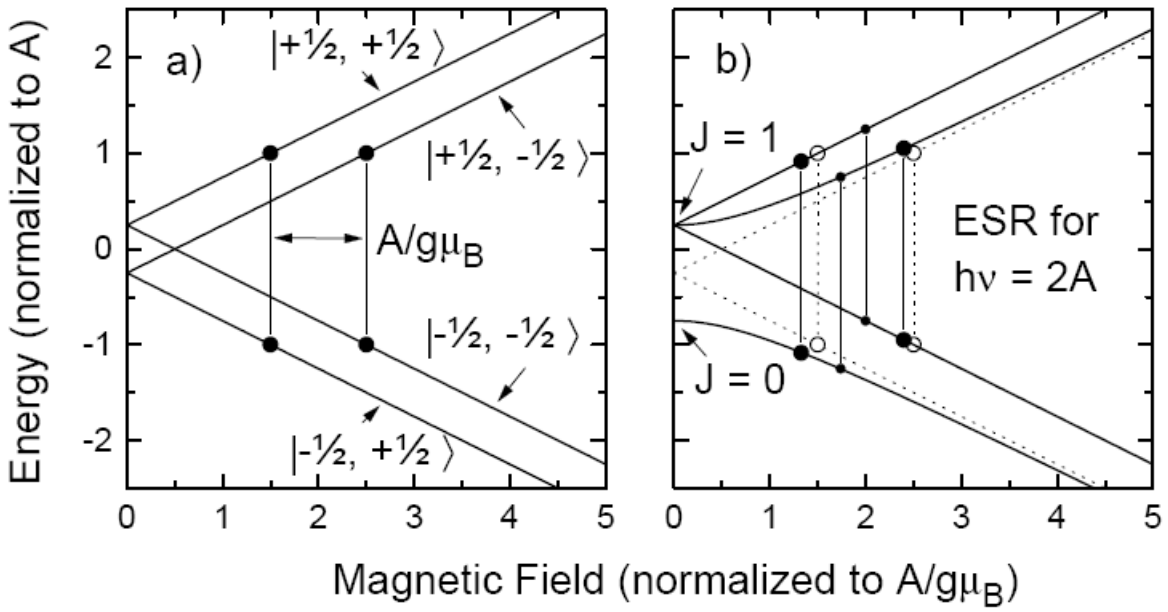

Fig. 1: *Breit-Rabi diagrams a) of the first-order solutions and b) of the exact solutions of the spin Hamiltonian of Eq. (12) with the electronic spin S = 1/2, the nuclear spin I = 1/2, and the hyperfine interaction A. For better comparison, the first-order solutions are included in b) with dashed lines. The energy levels are labelled according to the basis states* $|m_s, m_i\rangle$ *which are eigenstates of* $\mathbf{H}$ *at* $\mu_B Bg >> A$. *For* $\mu_B Bg << A$, *I tends to be coupled with S to an effective angular momentum J = S − I, … , S + I. The vertical lines indicate the two strongly allowed ESR transitions for a microwave energy hν = 2A. In (b), also the weakly allowed transitions are indicated.*

According to the dipole selection rules, the allowed electron spin resonance (ESR) transitions are those with $\left|+\frac{1}{2},\pm\frac{1}{2}\right\rangle \longleftrightarrow \left|-\frac{1}{2},\pm\frac{1}{2}\right\rangle$ with $\Delta m_s = \pm 1$ and $\Delta m_i = 0$. For a given transition energy $\Delta E = h\nu$, where *h* is the Planck constant, these two transitions appear at the magnetic fields $B = \left(h\nu \pm \frac{A}{2}\right)/\mu_B g$ in the first-order approximation. With the characteristic polynomial of the inner 2 × 2 block matrix, the exact energy eigenvalues $E_1, \ldots, E_4$ can be calculated analytically without approximations over the complete magnetic field range

$$E_{1,4} = +\frac{1}{4}A \pm \frac{1}{2}\mu_B Bg \tag{13}$$

$$E_{2,3} = -\frac{1}{4}A \pm \frac{1}{2}\sqrt{(\mu_B Bg)^2 + A^2} \quad . \tag{14}$$

The characteristic anti-crossing between the $\left|\pm\frac{1}{2},\mp\frac{1}{2}\right\rangle$ levels for small external fields is shown in Fig. 1 b). In the low-field regime, the eigen-vectors $\left|E_{2,3}\right\rangle$ are symmetric and antisymmetric combinations of the $\left|\frac{1}{2},-\frac{1}{2}\right\rangle$ and $\left|-\frac{1}{2},\frac{1}{2}\right\rangle$ basis vectors. As a consequence, the $\left|+\frac{1}{2},\pm\frac{1}{2}\right\rangle \longleftrightarrow \left|-\frac{1}{2},\mp\frac{1}{2}\right\rangle$ transitions are not completely "forbidden" in the low-field regime, as indicated with the smaller dots in Fig. 1 b). Physically, the system is then best described via a coupled angular momentum $J = S - I, \ldots, S + I$ for $\mu_B Bg \ll A$. For $A > 0$, the $J = 0$ singlet state with opposite nuclear and electronic spin orientation has lower energy than the "ferromagnetically" coupled $J = 1$ triplet state.

3 Device concepts

The original concept to use the electron spin and the nuclear spin of phosphorus donors in silicon as qubits goes back to Kane [18][19]. A device similar to the one envisaged by him is shown in Fig. 2. It consists of two phosphorus donors placed in isotopically pure ^{28}Si to suppress decoherence by the ^{29}Si nuclear spins present in natural silicon. Each donor is positioned below a separate gate, denoted A gate. In between the two donors and their respective A gates, a second gate denoted J is placed. The device is expected to operate at a temperature T of about 100 mK and at a magnetic field higher than 2 T, so that the electron spins will be fully polarized.

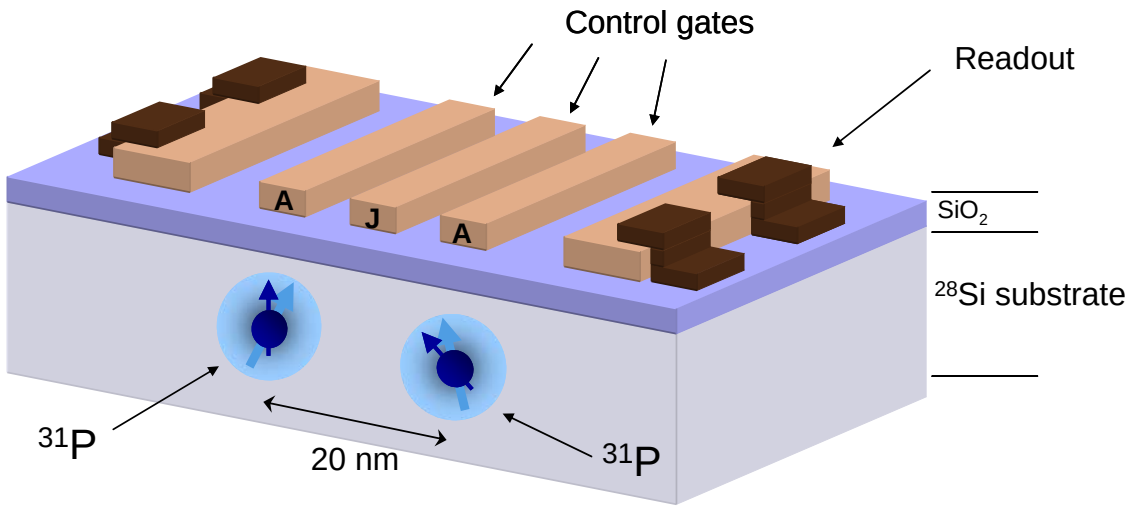

Fig. 2: *Kane concept for a quantum logic element based on the nuclear spins of ^{31}P donors in isotopically pure ^{28}Si.*

With the help of the A gate, the wave function of the donor electron can be manipulated, pulling it towards the Si/SiO_2-interface or pushing it away from it. The hyperfine interaction A between the two spins present in a single ^{31}P donor, the electron spin S and the nuclear spin I, is given by the so-called Fermi contact hyperfine interaction $A = \frac{2}{3}\mu_0 g \mu_B g_n \mu_n \left|\psi(0)\right|^2$,

where g_n is the nuclear g-factor of ^{31}P, μ_n the nuclear magneton and $|\psi(0)|^2$ the probability density of the electron donor wave function at the position of the nucleus [20][21]. Changes of the wave function due to a Stark effect should therefore lead to a variation of the hyperfine interaction. If electron spin resonance with $\Delta m_s=\pm 1$ is excited at the position of one of the hyperfine-split resonances, say $m_i=+1/2$, for a certain bias voltage at the A gate, changes of that bias voltage will lead to that particular electron spin transition going off resonance. Exciting the corresponding nuclear magnetic resonance (NMR) with $\Delta m_i = \pm 1$ effectively given by the hyperfine interaction A, a change of the bias voltage will similarly switch on or off the nuclear spin transition. Thereby, while exciting ESR or NMR globally, via the application of gate voltages either the electron or the nuclear spin can be addressed locally. This allows the realization of single qubit operations or gates. In his original proposal, Kane envisaged the use of the nuclear spins a qubits. A coupling of two nuclear spins at neighboring donors and therefore a two-qubit gate is possible via the electron spins at the respective donors. Their exchange interaction and thereby also the interaction between the nuclear spins are controlled in Fig. 1 by the coupling gate J influencing the overlap of the electronic wave functions. Since the exchange coupling, which dominates the spin-spin interaction of neighboring ^{31}P electrons, depends exponentially on the distance of the donor atoms, the accurate placement of the donors is quite crucial in this respect. To be able to effectively influence the coupling by a J gate, distances of about 5 to 10 Bohr radii are expected to be necessary.

The read-out of the electron spin state can similarly be discussed with the help of Fig. 2. For this, the gate voltages are adjusted such that the electron would be transferred from one donor to the other. Let us assume that we want to read-out the spin on the left and that the spin on the right is in a well known state such as spin down $m_s=-1/2$. The final state will be a double occupied donor state $^{31}P^-$, which according to the Pauli principle has to be in a total $S=0$ singlet state. The transfer of the electron between the donors can therefore only take place when the left electron is in a spin up state initially, or, more correctly, if the two electron spins also initially form a singlet. The Pauli principle therefore governs the charge transfer rate, so that the spin information is transferred into a charge information. Adiabatically changing the coupling of the two electron spins furthermore allows to convert the nuclear spin state into the spin symmetry of the electron spin pair, thereby facilitating the read-out of the nuclear spin. Finally, Kane suggests to use sensitive capacitive techniques such as radio-frequency single-electron transistors (rf-SETs) to determine the charge state of the read-out donor, the right donor in our case.

The effect of electric fields E on the hyperfine interaction of donors has been investigated in detail using ^{121}Sb [22]. Relative changes of the g-factor of $\Delta g/g=-1\text{x}10^{-5}\ \mu\text{m}^2/\text{V}^2\ E^2$ and of the hyperfine interaction of $\Delta A/A=-3.7\text{x}10^{-3}\ \mu\text{m}^2/\text{V}^2\ E^2$ have been found The application of high electric fields is limited by field ionization, so that only about 3 kV/cm can be used. This restricts the relative change in hyperfine interaction to about $3\text{x}10^{-4}$. The vicinity of the Si/SiO_2-interface will increase the applicable field somewhat, but still the Stark effect on the hyperfine interaction is limited.

The main advantage of the Kane concept based on the nuclear spins of the ^{31}P is their long coherence. The nutation rate with which spins can be flipped is given by $\nu_{nut} = g\mu_B B_1 / h$ or $\nu_{nut} = g_n\mu_n B_1 / h$, where B_1 is the strength of the microwave or radio-frequency magnetic field used to drive the ESR or NMR, respectively. For the same B_1 fields, electron spins can be

manipulated much faster than nuclear spins, allowing a higher clock speed in a possible quantum processor and simultaneously tolerating smaller T_2.

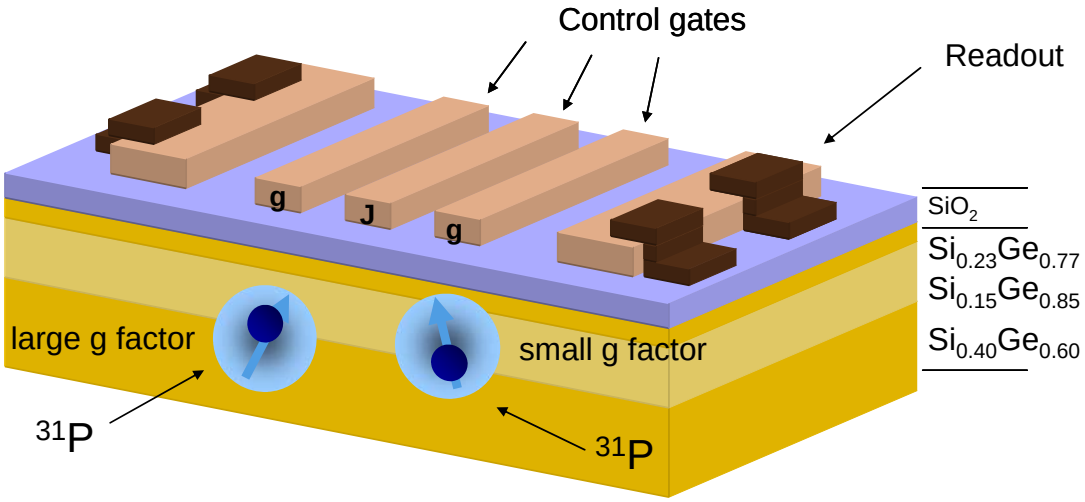

Fig. 3: *Proposal by Vrijen and coworkers on a quantum logic element based on donors placed at the interface of two epitaxial layers of SiGe with different alloy composition.*

Vrijen and coworkers suggested an alternative concept for a donor-based quantum logic element using the electron spins of donors placed at the interface of two different semiconductor materials as qubits (Fig. 3) [23]. The full miscibility of Si and Ge as well as the existence of stable nuclear spin-free Si and Ge isotopes renders the SiGe alloy system particularly interesting for this approach. Indeed, the g-factor of donors in Si is about 1.998, while in Ge a g of 1.563 is found. Therefore, placing a donor at the interface of two isotopically pure ^{28}Si and ^{70}Ge layers, or rather two isotopically pure $Si_{1-x}Ge_x$ alloys with alloy compositions such that the donor level is at the same energy in both layers, one might influence the g-factor via pushing or pulling the donor wave function from one material to the other with a gate now labeled g to a larger degree than by the Stark effect discussed for donors in pure Si above. However, it must be noted that the electrons will reside in different valleys in the two layers, since the conduction band minima of Si are near the X point in the Brillouin zone, while the band minima in Ge are at the L point. The effect of an effective intervalley scattering performed by the application of an electric field in the Vrijen concept in particular on T_2 remains to be investigated. Nevertheless, in addition to a possibly much higher change in the g-factor, the more shallow donors in Ge-rich SiGe alloys also have larger Bohr radii, so that the qubits have to be farther apart than in the pure Si design by Kane and the requirements for the accuracy of the donor placement can be less stringent.

4 Fabrication of single-donor devices

One of the main challenges in the realization of donor-based quantum logic devices is the accurate placement of single donors. As outlined above, the distance of the donors both to the Si/SiO_2-interface and to the neighboring donors should be typically of the order of 20 nm. The main approaches to realize such a position of single donor atoms are implantation and lithography.

In state-of-the-art single-dopant implantation, the silicon substrate itself is used as a particle detector [24]. Phosphorus ions being implanted will generate electron-hole pairs, which are separated in the applied electric field. Using appropriate electronics, the current pulse thus generated by a single ion implantation event can be detected. If a low flux of incident ions is used, a beam blanker can be activated quickly enough after the observation of an implantation event to prevent further ions from reaching the substrate, allowing single ion implantations. Lithographically-defined masks can define the location of the implantation. When pairs of dopants are to be formed, the approach based on two neighboring openings in the mask will provide such dopant pair structures with a probability of 50%. Alternatively, atomic force microscopy (AFM) tips, which have a channel in the tip through which the ions can be implanted, have been used as moveable implantation masks [25], reducing the risk of double implantation through a single opening in the lithographically-defined mask.

Shallow implantations with a typical depth of 20 nm can be obtained with phosphorus ion energies of the order of 10 to 20 keV. However, the scattering between the incident ion and the atoms of the Si substrate lead to straggle. At a primary energy of 14 keV for singly negatively charged P ions, the exact position of the P atom in the Si substrate after implantation varies by about 11 nm in the distance to the substrate surface and by about 8 nm in the directions perpendicular to that. Together with the diameter of the mask openings, this straggle leads to a variation of the distance between P atoms e.g. forming a quantum logic element as sketched in Fig. 2 by several Bohr radii.

An alternative, but experimentally even more challenging approach is the use of lithography based on scanning tunneling microscopy (STM) [26][27][28]. The fundamental idea is to fabricate a hydrogen-terminated surface and, with the help of an STM tip, to locally remove this atomic analog to a photoresist. The surface Si atoms not terminated by hydrogen are very reactive, and PH_3 molecules brought onto the surface will bind to them, which allows to position single phosphorus atoms with the atomic precision of STM. It only remains to form an epitaxial Si cap layer, followed by growth of a SiO_2 barrier and the fabrication of the gate contacts. However, Si tends to move with the growth front at the temperatures usually used for high quality epitaxial growth, which would significantly reduce the accuracy of the P placement in the final device structure. Using an intermediate growth step at room temperature, followed by a rapid thermal anneal and a high temperature overgrowth, the "straggle" in the P position can be reduced to below 1 nm, a value smaller than the Bohr radius of effective mass donors in Si. However, it should be noted that also in the case of STM lithography, every P donor pair formed will have such a different overlap of the wave functions that the relevant voltages at the J gates in Fig. 2 for the switching of the electronic spin-spin interaction will have to be adjusted separately for each pair. Apart from devices for quantum information processing, the STM-based lithography summarized also allows the fabrication of other interesting and novel devices for "atomic electronics" in general.

5 Read-out of electron spin states

The second main challenge is the read-out of single donor spins. While this has been demonstrated for electrostatically-defined [4] and self-organized quantum dots [29] as well as for the NV-center in diamond [30], the successful determination of both the electron and the nuclear spin state of single donors is subject to intense work by several groups.

5.1 Silicon rf-SETs

In parallel to the fabrication of single dopant devices, significant progress is being made in the development of techniques for the sensing of single charges in Si devices, an integral step in the measurement of spin states. An example are radio-frequency single electron transistor (rf-SET) formed at the Si/SiO_2-interface of a nearly undoped Si substrate [31]. Between the source and drain contacts, an n-type channel with a low electron density is formed. Via two gate electrodes, an island can be controllably created in the middle of the channel. The radio-frequency reflectance of the device, a measure of the source-drain conductance, shows clear Coulomb diamonds, demonstrating the possibility to measure the change of the number of charges on the islands on a single-electron level. The particular detection via rf reflectance allows charge measurements with a bandwidth as high as 2 MHz, comparable to that of mature aluminium rf-SETs. These results suggest that the quantum logic element as well as the charge detector required for the spin read-out could be fabricated as an integrated device from Si.

5.2 Spin-to-charge conversion at the Si/SiO_2-interface

So far, we have discussed the read-out of the electron spin state via a spin-to-charge conversion process involving two neighboring ^{31}P donor states. However, any paramagnetic state can be used as a partner to read-out the donor spin state. To be able to manipulate the qubits, the donors have to be near to the gate electrodes, which are insulated from the silicon substrate via an oxide. At the interface of the silicon and this oxide, defects such as unsaturated Si "dangling" bonds occur naturally in concentrations of typically between 10^{11} and 10^{13} cm^{-2}, depending on the exact oxide growth conditions. By passivation with hydrogen in a forming gas anneal or via compensation, the density of these defects can be reduced. However, they can also be used very conveniently as the partner required for spin-to-charge conversion [32].

Figure 4 shows a spin-dependent recombination process involving a ^{31}P donor electron and the dominant Si/SiO_2-interface defect named P_{b0} [33]. As in the case of the charge transfer between neighboring P donors discussed above, the recombination step can only proceed if the ^{31}P-P_{b0} pair is initially in a singlet spin configuration. In this case, a negatively charged P_{b0}^- state is formed. If mobile charge carriers are present such as electrons and holes generated by illumination, an electron will be trapped by the positively charged ^{31}P and a hole by the negatively charged P_{b0} center, leading to a reduction of the carrier densities and to a reduction of the conductivity. The symmetry of the spin pair and therefore also the electron spin state of the donor can thus be detected by changes in e.g. the photoconductivity.

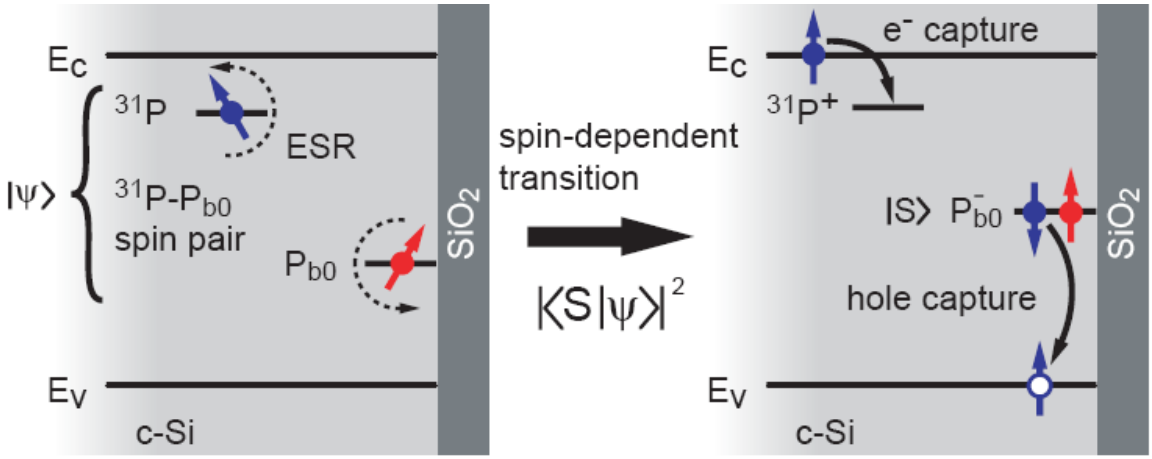

Fig. 4: *Spin-to-charge conversion at the Si/SiO_2-interface.*

To demonstrate the feasibility of this electrical read-out scheme of the electron spin state, let us look at an ensemble of ^{31}P-P_{b0} pairs. Due to the spin-allowed recombination, most ^{31}P-P_{b0} singlet pairs will have recombined in thermal equilibrium, most ^{31}P-P_{b0} pairs remaining will be in a triplet configuration. Turning triplets into singlets via electron spin resonance of either the ^{31}P or the P_{b0} (which is possible when the ^{31}P-P_{b0} coupling is small), pair recombination is increased [3]. Continuous resonance excitation will lead to a continuous oscillation of the ensemble being dominantly in the triplet or singlet configuration and, simultaneously, an oscillation of the ^{31}P-P_{b0} recombination rate. The observation of these Rabi oscillations in the conductivity will be a clear demonstration of this spin read-out concept. However, the *RC*-timeconstants of the samples typically studied do not allow the direct monitoring of these oscillations. To overcome this limitation, two technical tricks summarized in Fig. 5 are currently used [34].

Figure 5 a) shows the oscillation of the recombination during the application of a microwave pulse exciting electron spin resonance of either partner in the spin pair. After the pulse, the spin system is most-likely in a non-equilibrium state determined by the symmetry of the ^{31}P-P_{b0} pairs and will relax back into equilibrium. Governed by different time constants including the singlet- and triplet recombination times and the *RC*-timeconstant of the detection system, a current transient will be observed during this relaxation. The amplitude of this current transient, however, is proportional to the deviation of the singlet/triplet content of the spin pair ensemble at the end of the microwave pulse from thermal equilibrium (Fig. 5 b), so that measurements of this transient long after the excitation of the spin resonance has finished provide the wanted information on the spin orientation [34]. To further improve the signal-to-noise ratio of these experiments, the current transient is integrated over a certain time window, yielding a charge *Q* as the primary physical quantity measured (Fig. 5 c).

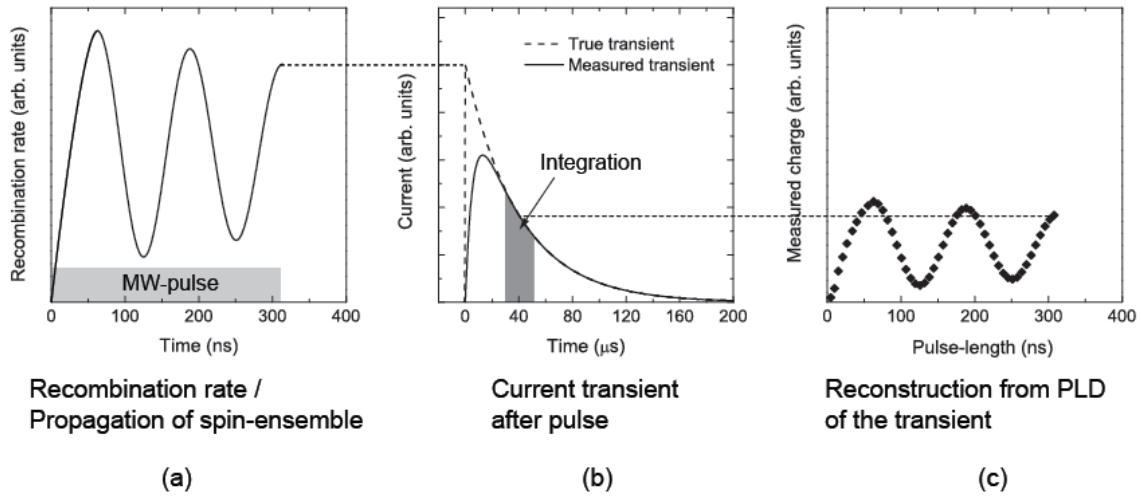

Fig. 5: *Measurement of the recombination rate at the end of the microwave pulse exciting the electron spin resonance of ^{31}P-P_{b0} pairs.*

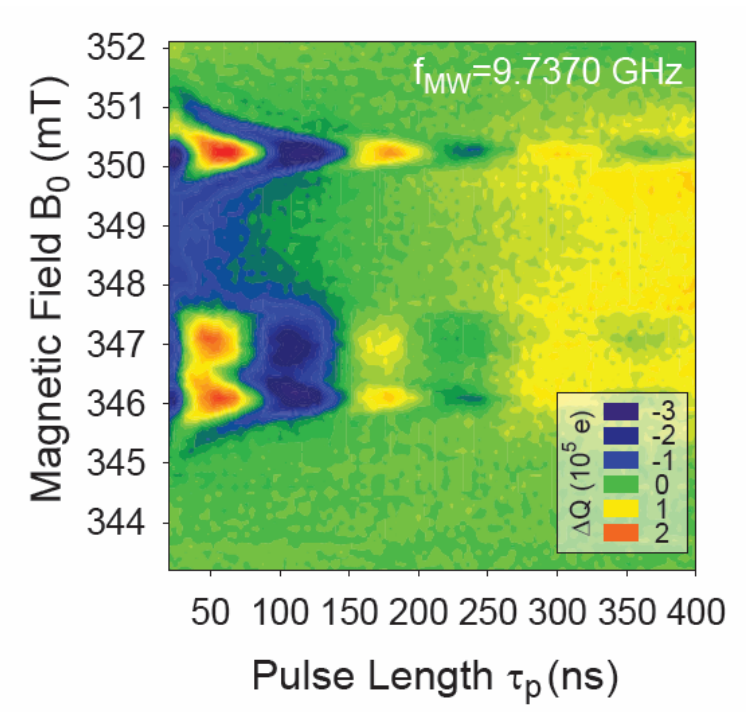

Fig. 6: *Rabi oscillations of the ^{31}P-P_{b0} recombination at the Si/SiO_2-interface observed by electrically detected magnetic resonance (EDMR).*

The result of such pulsed electrically detected magnetic resonance (EDMR) experiments are shown in Fig. 6 as a function of the length of the microwave pulse τ_p for a sample containing about 10^{10} P donors in a 15 nm thin Si layer capped with a native SiO_2, corresponding to a phosphorous concentration of about 10^{17} cm^{-3}. At three different magnetic fields, clear oscillations of Q are found [32]. The resonances at 346.1 and 350.3 mT are the hyperfine split signature of the ^{31}P donor. The difference in the magnetic fields of the two resonance positions is $A/\mu_B g$ as shown in Fig. 1. The resonance at 347 mT is caused by the P_{b0} centers. Final proof that indeed Rabi oscillations induced by magnetic resonance are observed comes

from the reduction in the Rabi oscillation frequency $\nu_{nut} = g\mu_B B_1 / h$ upon lowering of the microwave power $P_{\mu w} \propto B_1^2$ used (Fig. 7).

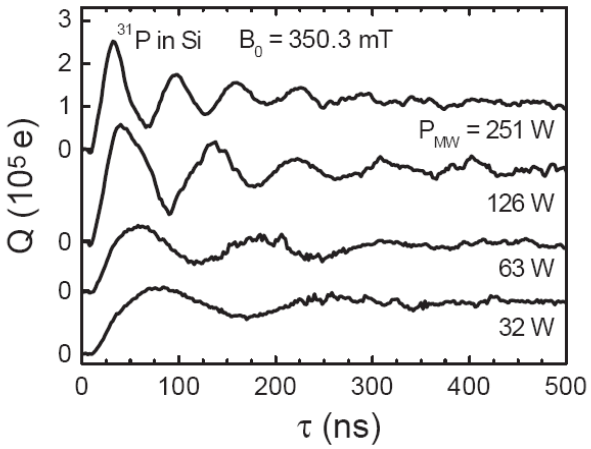

Fig. 7: *Dependence of the Rabi oscillation frequency on the microwave power used.*

5.3 Decoherence

Spin coherence can be studied with a variety of different techniques, including the measurement of the spin resonance lineshape and intensity as a function of microwave power and dynamical variables such as the rate with which the magnetic field is changed. These approaches can be summarized by the term "passage effects". Alternatively, so-called echo techniques can be used [35]. The coherence time T_2 can e.g. be determined via a Carr-Purcell echo experiment, which consists of a pulse sequence denoted by $\pi/2$-τ_1-π-τ_2, where $\pi/2$ and π denote the rotation angle of the spin system induced by resonant microwave pulses and τ_1 and τ_2 are the free evolution periods between the pulses [36]. Such a Carr-Purcell echo is shown in Fig. 8 a) for an ensemble of identical spins (e.g., the spins of phosphorus donors) plotted in a Bloch sphere, starting, e.g., with the spin ensemble in the down eigenstate m_s=-1/2. The microwave pulses are assumed to rotate the spins around the *x*-axis of the Bloch sphere. The echo develops in the *x*-*y* plane of the Bloch sphere, giving rise to a pulse in the transverse magnetization at $\tau_1=\tau_2$, which is easily detectable in conventional ESR. However, the ^{31}P-P$_{b0}$ spin-to-charge conversion process is sensitive to the singlet-triplet symmetry of a spin pair, which is not changed by the formation of an echo in the transverse magnetization. A successful detection of such echoes via charge transport therefore requires so-called echo tomography [37], where after the second free evolution period τ_2 a final $\pi/2$ pulse rotates the spin system back into singlet or triplet eigenstates of the pair, shown in Fig. 8 c) in more detail. For $\tau_2<\tau_1$ and $\tau_2>\tau_1$, no echo has developed in the *x*-*y* plane so that after the final $\pi/2$ pulse, the spins of the ensemble point to all directions in the *x*-*z* plane of the Bloch sphere. Both triplet and singlet configurations will therefore be found in ensembles of the ^{31}P-P$_{b0}$ spin pairs under these conditions. However, for $\tau_2=\tau_1$, an echo has developed, so that after the final $\pi/2$ pulse, the ^{31}P spin ensemble is in the original m_s=-1/2 down eigenstate again. If the P$_{b0}$ partner in the spin state is in its m_s=-1/2 state, we find only the triplet configuration for the ^{31}P-P$_{b0}$ spin pairs. Therefore, echoes can be formed also in the singlet-triplet symmetry of spin pairs and are accessible to purely electrical detection.

We can predict the experimental signature of the echoes. The pulse sequence $\pi/2$-τ_1-π-τ_2-$\pi/2$ contains microwave pulses with a total length of 2π. Ideally, we therefore expect a value of *Q*

after a Carr-Purcell echo sequence with $\tau_2=\tau_1$ equal to the Q found after a rotation by 2π in a Rabi-flop experiment shown in Fig. 8 b). For $\tau_2<\tau_1$ and $\tau_2>\tau_1$, the spin-pairs are not in the steady-state configurations. Rather, the ensemble of spin-pairs will contain singlet and triplet configuration in about equal contributions and therefore a larger Q corresponding to Rabi oscillations by $3\pi/2$ and $5\pi/2$ is expected as the result of such Carr-Purcell sequences. A quantitative comparison of Q observed on the high-field ^{31}P resonance at 350.3 mT during the echo in Fig. 8 d) to the Q observed in the Rabi oscillation in Fig. 8 b) demonstrates that the echo amplitude ΔQ is indeed as large as expected.

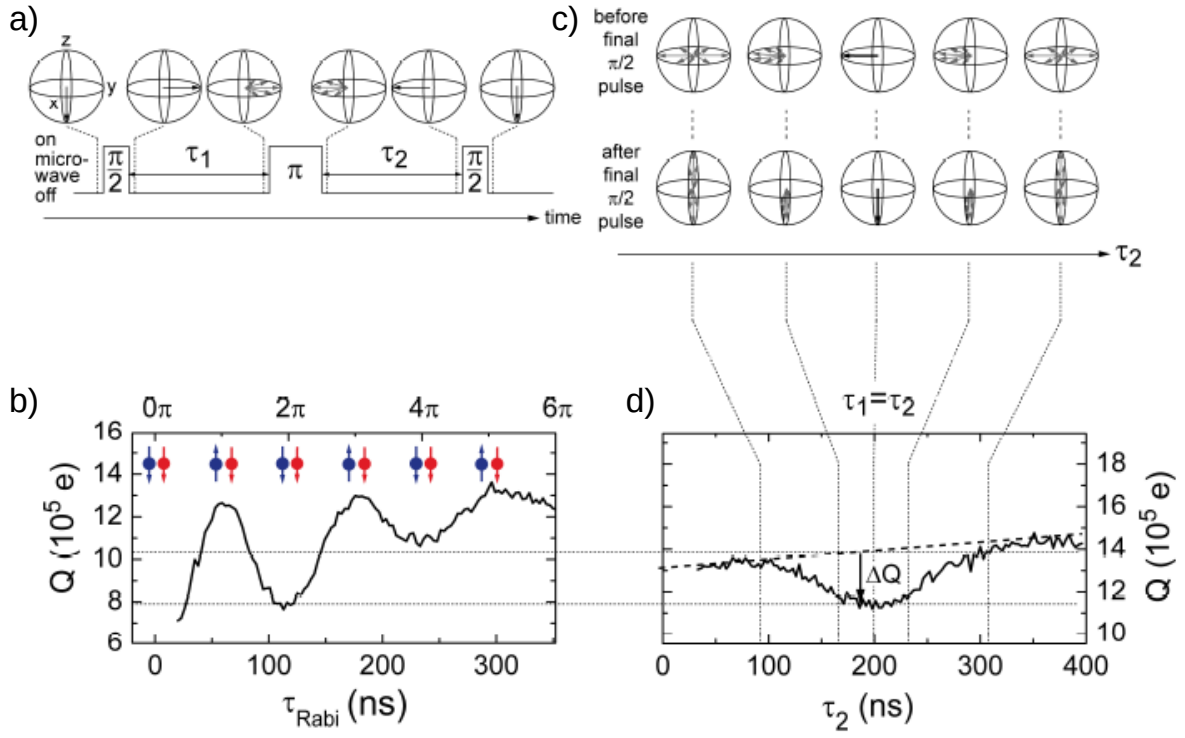

Fig. 8: *Application of echo tomography to the Carr-Purcell method to measure the coherence of ^{31}P-P_{b0} spin pairs via charge transport. b) and d) show that the echo amplitude ΔQ can be understood quantitatively from the amplitude of the Rabi oscillations.*

To determine the echo decay time and therefore the effective coherence time, the echo sequence is measured as a function of τ_1 and τ_2. In all cases, the echo is observed at $\tau_2=\tau_1$ and its intensity decreases monoexponentially for longer values of τ with a characteristic time constant of about 1.7 µs both for echos detected on the ^{31}P and the P_{b0} resonance [37]. We have already mentioned the much longer values for T_2 observed in bulk crystals of isotopically pure ^{28}Si with low ^{31}P concentrations [8]. In bulk ^{nat}Si with a donor concentration of 10^{17} cm^{-3} as in our samples, the T_2 determined by magnetization echo experiments is already reduced to about 10 µs [38]. The presence of the Si/SiO_2-interface is also expected to lead to a reduction of the coherence [39], as has been shown experimentally for implanted Sb donors [40]. However, EDMR experiments using pulses at different microwave frequencies to induce spin flips of both partners in the ^{31}P-P_{b0} pair are able to measure the singlet

recombination time. A quantitative comparison of the singlet recombination time and the effective echo decay time shows that the coherence of the ^{31}P-P_{b0} is limited by the lifetime of the spin pair, rather than by spin-spin scattering. The observation of spin echos in the charge transport opens the possibility to apply pulse sequences such as DEER and ESEEM including free evolution times to study spin-spin interactions in these devices, allowing the determination of the coupling between the electron spins at ^{31}P and P_{b0} or between the donor electron spin and the nuclear spins of ^{29}Si, respectively, and ultimately the realization of entanglement between these spins.

5.4 Outlook

The results discussed above show that, at least for ensembles, the read-out of the electron spin state via ^{31}P-P_{b0} pairs is feasible. This observation opens up a wealth of opportunities: Using the A gates in Fig. 2, it can be envisaged that by changing the gate voltages the coupling between the donor wave function and the read-out spin at the Si/SiO_2-interface can be varied, which would allow the selective addressing and reading of the single ^{31}P spins [41]. Electrical detection of spin resonance, but not yet actual spin read-out has already been achieved on samples containing as few as 50 P donors [42]. Furthermore, several different approaches for the electrical read-out of the nuclear spin state are being discussed. Irrespective of the possible use of this particular read-out scheme or even the use of donors for quantum information processing, these studies allow a more detailed understanding of the complex charge carrier and spin dynamics in semiconductor nanostructures.

Acknowledgements

I would like thank my current and former students H. Huebl, A. Stegner, F. Hoehne, J. Lu, B. Grolik, B. Galler, L. Dreher and C. Bihler for discussions and their dedicated work in the lab. In fact, most should be coauthors of this contribution. This holds especially for T. Graf, who originally wrote Sec. 2 for his PhD thesis [43]. However, all errors are mine. The initial investigations on the read-out of donor electron spin states were performed in collaboration with K. Lips and C. Böhme. Discussions with S. Angus, R. Clark, A. Dzurak, A. Ferguson, W. Hutchison, K. Itoh, D. Jamieson, D. McCamey, S. McKibbin, S. Rogge, T. Schenkel and M. Simmons are gratefully acknowledged. The research into donor spin physics at the Schottky Institut is funded by Deutsche Forschungsgemeinschaft through SFB 631.

References

[1] D. P. DiVincenzo, Fortschr. Phys. **48**, 771 (2000)
[2] L. M. K. Vandersypen and I. L. Chuang, Rev. Mod. Phys. **76**, 1037 (2004)
[3] A modern introduction into magnetic resonance is e.g. M. H. Levitt, *Spin Dynamics* (Wiley, Chichester, 2001)
[4] J. M. Elzerman, R. Hanson, L. H. Willems van Beveren, B. Witkamp, L. M. K. Vandersypen and L. P. Kouwenhoven, Nature **430**, 431 (2004)
[5] J. R. Petta, A. C. Johnson, J. M. Taylor, E. A. Laird, A. Yacoby, M. D. Lukin, C. M. Marcus, M. P. Hanson and A. C. Gossard, Science **309**, 2180 (2005)
[6] M. Kroutvar, Y. Ducommun, D. Heiss, M. Bichler, D. Schuh, G. Abstreiter and J. J. Finley, Nature **432**, 81 (2004)
[7] G. Feher and E. A. Gere, Phys. Rev. **114**, 1245 (1959)
[8] A. M. Tyryshkin, J. J. L. Morton, S. C. Benjamin, A. Ardavan, G. A. D. Briggs, J. W. Ager and S. A. Lyon, J. Phys. Condens. Matter **18**, S783 (2006)
[9] J. J. L. Morton, A. M. Tyryshkin, R. M. Brown, S. Shankar, B. W. Lovett, A. Ardavan, T. Schenkel, E. E. Haller, J. W. Ager and S. A. Lyon, Nature **455**, 1085 (2008)
[10] E. Abe, K. M. Itoh, J. Isoya and S. Yamasaki, Phys. Rev. B **70**, 033204 (2004)
[11] N. Shaji, C. B. Simmons, M. Thalakulam, L. J. Klein, H. Qin, H. Luo, D. E. Savage, M. G. Lagally, A. J. Rimberg, R. Joynt, M. Friesen, R. H. Blick, S. N. Coppersmith, M. A. Eriksson, Nature Phys. **4**, 540 (2008)
[12] L. Childress, M. V. Gurudev Dutt, J. M. Taylor, A. S. Zibrov, F. Jelezko, J. Wrachtrup, P. R. Hemmer and M. D. Lukin, Science **314**, 281 (2006)
[13] http://lukin.physics.harvard.edu/Theses/LilyThesis.pdf
[14] J. A. Weil, J. R. Bolton and J. E. Wertz, *Electron paramagnetic resonance* (Wiley, New York, 1994)
[15] C. Rudowicz, Magn. Reson. Rev. **13**, 1 (1987)
[16] J. J. Sakurei, *Modern quantum mechanics* (Addison-Wesley, New York, 1994)
[17] J. W. Orton, *Electron paramagnetic resonance* (Iliffe Books, London, 1968)
[18] B. E. Kane, Nature **393**, 133 (1998)
[19] B. E. Kane, Fortschr. Phys. **48**, 1023 (2000)
[20] F. Feher, Phys. Rev. **114**, 1219 (1959)
[21] H. Huebl, A. R. Stegner, M. Stutzmann, M. S. Brandt, G. Vogg, F. Bensch, E. Rauls, and U. Gerstmann, Phys. Rev. Lett. **97**, 166402 (2006)
[22] F. R. Bradbury, A. M. Tyryshkin, G. Sabouret, J. Bokor, T. Schenkel and S. A. Lyon, Phys. Rev. Lett. **97**, 176404 (2006)
[23] R. Vrijen, E. Yablonovitch, K. Wang, H. W. Jiang, A. Balandin, V. Roychowdhury, T. Mor and D. DiVincenzo, Phys. Rev. A **62**, 012306 (2000)
[24] D. N. Jamieson, C. Yang, T. Hopf, S. M. Hearne, C. I. Pakes, S. Prawer, M. Mitic, E. Gauja, S. E. Andresen, F. E. Hudson, A. S. Dzurak and R. G. Clark, Appl. Phys. Lett. **86**, 202101 (2005)
[25] A. Persaud, F. I. Allen, F. Gicquel, S. J. Park, J. A. Liddle, T. Schenkel, Tzv. Ivanov, K. Ivanova, I. W. Rangelow and J. Bokor, J. Vac. Sci. Technol. B **22**, 2992 (2004)
[26] S. R. Schofield, N. J. Curson, M. Y. Simmons, F. J. Rueß, T. Hallam, L. Oberbeck, and R. G. Clark, Phys. Rev. Lett. **91**, 136104 (2003)
[27] K. E. J. Goh, L. Oberbeck, M. Y. Simmons, A. R. Hamilton and R. G. Clark, Appl. Phys. Lett. **85**, 4953 (2004)
[28] T. Hallam, T. C. G. Reusch, L. Oberbeck, N. J. Curson and M. Y. Simmons, J. Appl.

Phys. **101**, 034305 (2007)
[29] J. Berezovsky, M. H. Mikkelsen, O. Gywat, N. G. Stoltz, L. A. Coldren and D. D. Awschalom, Science **314**, 1916 (2006)
[30] F. Jelezko, T. Gaebel, I. Popa, A. Gruber and J. Wrachtrup, Phys. Rev. Lett. **92**, 076401 (2004)
[31] S. J. Angus, A. J. Ferguson, A. S. Dzurak and R. G. Clark, Appl. Phys. Lett. **92**, 112103 (2008)
[32] A. R. Stegner, C. Boehme, H. Huebl, M. Stutzmann, K. Lips and M. S. Brandt, Nature Phys. **2**, 835 (2006)
[33] E. H. Poindexter, P. J. Caplan, B. E. Deal and R. R. Razouk, J. Appl. Phys. **52**, 879 (1981)
[34] C. Boehme and K. Lips, Phys. Rev. B **28**, 245105 (2003)
[35] A good introduction into pulse sequences can be found in R. Freeman, *Spin Choreography* (Oxford Univ. Press, Oxford, 1998)
[36] H.Y. Carr and E. M. Purcell, Phys. Rev. **94**, 630 (1954)
[37] H. Huebl, F. Hoehne, B. Grolik, A. R. Stegner, M. Stutzmann and M. S. Brandt, Phys. Rev. Lett. **100**, 177602 (2008)
[38] M. Chiba and A. Hirai, J. Phys. Soc. Jpn. **33**, 730 (1972)
[39] R. de Sousa, Phys. Rev. B **76**, 245306 (2007)
[40] T. Schenkel, J. A. Liddle, A. Persaud, A. M. Tyryshkin, S. A. Lyon, R. de Sousa and K. B. Whaley, Appl. Phys. Lett. **88**, 112101 (2006)
[41] A. R. Stegner, C. Boehme, H. Huebl, M. Stutzmann, K. Lips and M. S. Brandt, arXiv:quant-ph/0607178 (2006)
[42] D. R. McCamey, H. Huebl, M. S. Brandt, W. D. Hutchison, J. C. McCallum, R. G. Clark, and A. R. Hamilton, Appl. Phys. Lett. **89**, 182115 (2006)
[43] http://mediatum2.ub.tum.de/download/602968/602968.pdf